

# Analysis of NaN Divergence in Training Monocular Depth Estimation Model

Bum Jun Kim  
POSTECH

kmbmjn@postech.ac.kr

Hyeonah Jang  
POSTECH

hajang@postech.ac.kr

Sang Woo Kim  
POSTECH

swkim@postech.ac.kr

## Abstract

*The latest advances in deep learning have facilitated the development of highly accurate monocular depth estimation models. However, when training a monocular depth estimation network, practitioners and researchers have observed not a number (NaN) loss, which disrupts gradient descent optimization. Although several practitioners have reported the stochastic and mysterious occurrence of NaN loss that bothers training, its root cause is not discussed in the literature. This study conducted an in-depth analysis of NaN loss during training a monocular depth estimation network and identified three types of vulnerabilities that cause NaN loss: 1) the use of square root loss, which leads to an unstable gradient; 2) the log-sigmoid function, which exhibits numerical stability issues; and 3) certain variance implementations, which yield incorrect computations. Furthermore, for each vulnerability, the occurrence of NaN loss was demonstrated and practical guidelines to prevent NaN loss were presented. Experiments showed that both optimization stability and performance on monocular depth estimation could be improved by following our guidelines.*

## 1. Introduction

Understanding a driving scene is an important task for self-driving or advanced driver-assistance systems. In particular, constructing 3D scene information in a driving environment is crucial. To this end, studying monocular depth estimation, which aims to obtain the physical depth information from a single RGB image, is of paramount importance. Recently, deep neural networks [8, 9, 17, 37] have been extensively used, and they have also been incorporated into the monocular depth estimation task, in which a deep neural network is trained by the iterative optimization of gradient descent using a large dataset of RGB-LiDAR image pairs. The latest advances in deep learning have allowed us to develop a highly accurate monocular depth estimation model that is close to real-world applications.

However, the training of monocular depth estimation models has stability issues. When training a monocular

depth estimation model, practitioners and researchers have observed not a number (NaN) loss, which indicates a failure mode where the optimization diverged owing to inappropriate computations, such as division by zero. Several practitioners have reported NaN loss and difficulties in re-implementing monocular depth estimation models in the official GitHub repositories. When training a monocular depth estimation model, the optimization can either finish normally or lead to a NaN loss, even with the same model and hyperparameter setup. NaN losses have been reported to occur during the early training phase, as well as the late training phase near the optimal point. The stochastic and mysterious occurrence of the NaN loss has been a cause of concern among practitioners and researchers because it wastes time and resources.

It should be noted that NaN loss occurs rarely for other training tasks such as semantic segmentation, while it occurs frequently for the training task of monocular depth estimation. The root cause of the NaN loss has not been discussed in the literature and remains unclear. Determining the root cause is challenging as it requires debugging the training procedure of the deep neural network. Thus, currently, further research is required to reveal the root cause of NaN loss in training monocular depth estimation models. This is expected to overcome the instability of optimization, and thereby facilitate the research community and practitioners.

In this paper, we report an in-depth analysis that focuses on the occurrence of NaN loss when training a monocular depth estimation model. We thoroughly inspected the current implementations of monocular depth estimation networks, and discovered three types of vulnerabilities in their gradient descent optimization:

- First, the use of the square root loss, which is a common practice, yields an exploding gradient when approaching an optimal point. We discuss square root loss and its potential advantages and disadvantages.
- Second, the log-sigmoid function used in the monocular depth estimation network has numerical stability issues and is prone to NaN loss. This problem can be addressed either through careful weight initialization or by improv-

ing the numerical stability of the logarithmic function. To this end, we present a stable initialization range that assures the absence of NaN loss.

- Finally, a critical error exists in the implementation of variance computation, where half of the current implementations of monocular depth estimation models have potential problems. In a practical scenario, we demonstrated the accidental occurrence of NaN loss caused by this vulnerability.

For each vulnerability, we analyzed detailed computations and empirically demonstrated the occurrence of NaN through several simulations. We also provide practical guidelines for solving the NaN loss for each vulnerability.

## 2. Vulnerability Report

**Background and Formulation** This study considers the standard framework for supervised learning of the monocular depth estimation model. Let  $\mathbf{I} \in \mathbb{R}^{n_h \times n_w \times n_c}$  be an input image for a monocular depth estimation model, where  $(n_h \times n_w)$  is the size of the image and  $n_c$  represents the number of channels. The objective of monocular depth estimation is to generate a depth map  $\mathbf{y} \in \mathbb{R}^{n_h \times n_w}$  that estimates physical distance  $y_i$  for the  $i$ -th pixel in the image and exhibits a small error with its ground-truth  $\mathbf{y}^*$ . A deep neural network composed of an encoder and decoder with a head is used as the monocular depth estimation model that outputs  $\mathbf{y}$  from the input image  $\mathbf{I}$ . The monocular depth estimation task has constraints on the maximum depth  $M$  in meters, such as  $0 < y_i < 80$ , with  $M = 80$ . To generate a depth map with a constrained depth range, a sigmoid head with a max scaler has been commonly used as  $y_i = Mp_i = Ms(z_i)$ , where  $p = s(z) = 1/(1 + e^{-z})$ . Here,  $\mathbf{z} \in \mathbb{R}^{n_h \times n_w}$  is obtained using the last convolutional layer of the decoder  $\mathbf{z} = \mathbf{W}\mathbf{x} + b$ , where  $\mathbf{x} \in \mathbb{R}^{n_h \times n_w \times n_{in}}$ ,  $\mathbf{W} \in \mathbb{R}^{k_h \times k_w \times n_{in} \times 1}$ , and  $b \in \mathbb{R}$ .

Monocular depth estimation is a regression task aimed at obtaining real value predictions. However, opposed to common regression tasks, describing relative farness and nearness is more important in this task. Considering this task property, Eigen et al. [10] proposed scale-invariant log loss  $D$  as follows:

$$D = \frac{1}{n} \sum_i d_i^2 - \frac{\lambda}{n^2} \left( \sum_i d_i \right)^2, \quad (1)$$

where  $d_i = \log y_i - \log y_i^*$ ,  $\lambda \in [0, 1]$ , and  $n$  denotes the number of valid pixels. The scale-invariant log loss and its gradient do not depend on the maximum depth  $M$  and are suitable for reflecting relative farness and nearness. The monocular depth estimation network is optimized by minimizing the scale-invariant log loss, ideally to zero.

In practice, Lee et al. [22] proposed alternatively minimizing the square root of the scale-invariant log loss as fol-

lows:

$$L = \sqrt{D}. \quad (2)$$

They empirically observed that the use of the square root loss led to better performance. Since its introduction, square root loss has been widely employed in monocular depth estimation networks [26, 30, 35, 39, 40].

### 2.1. Vulnerability in Square Root Loss

However, we found that the square root loss caused NaN divergence. This problem arises from the unstable gradient of the square root loss. For weight  $\mathbf{W}$ , the gradient descent minimizing square root loss  $L$  with learning rate  $\eta$  can be expressed as follows:

$$\mathbf{W} \leftarrow \mathbf{W} - \eta \frac{\partial L}{\partial \mathbf{W}}, \quad (3)$$

$$\frac{\partial L}{\partial \mathbf{W}} = \frac{\partial L}{\partial D} \frac{\partial D}{\partial \mathbf{W}} = \frac{1}{2\sqrt{D}} \frac{\partial D}{\partial \mathbf{W}}. \quad (4)$$

By contrast, when using the scale-invariant log loss  $D$  for the minimization objective of the gradient descent, the gradient is  $\partial D / \partial \mathbf{W}$ . Thus, compared with scale-invariant log loss  $D$ , the use of square root loss  $L$  causes scaling of the gradient by  $1/2\sqrt{D}$ .

**Pros** The use of square root loss may help with optimization during the early training phase. In the early training phase, if the optimization is at an unstable point with a large loss and gradient, the use of square loss leads to a smaller gradient by a large  $D$ . This behavior reduces the large weight updates, similar to gradient clipping [33, 50], thereby preventing unstable optimization. Furthermore, to avoid overfitting to the training set, preventing zero loss and maintaining suboptimal loss during training is crucial since training and test losses differ in a strict sense [12, 24]. Considering this property, the use of square root loss may be beneficial to avoid overfitting to the training set and produce a type of regularization effect.

**Cons** The serious vulnerability of the square root loss arises during the late training phase, when the loss is suitably minimized. Note that the objective of the monocular depth estimation task is to achieve  $\mathbf{y} \rightarrow \mathbf{y}^*$  and  $D \rightarrow 0$  as much as possible. However, as  $D$  approaches zero, owing to the presence of  $\sqrt{D}$  in the denominator, the gradient becomes larger, which causes a deviation from the optimal point and disrupts the optimization. Even if  $D = 0$  is achieved by any methods, it causes NaN loss.

**Simulation** We empirically demonstrate the vulnerability of square root loss. We generated artificial random normal data, whose ground-truth followed the mean and standard

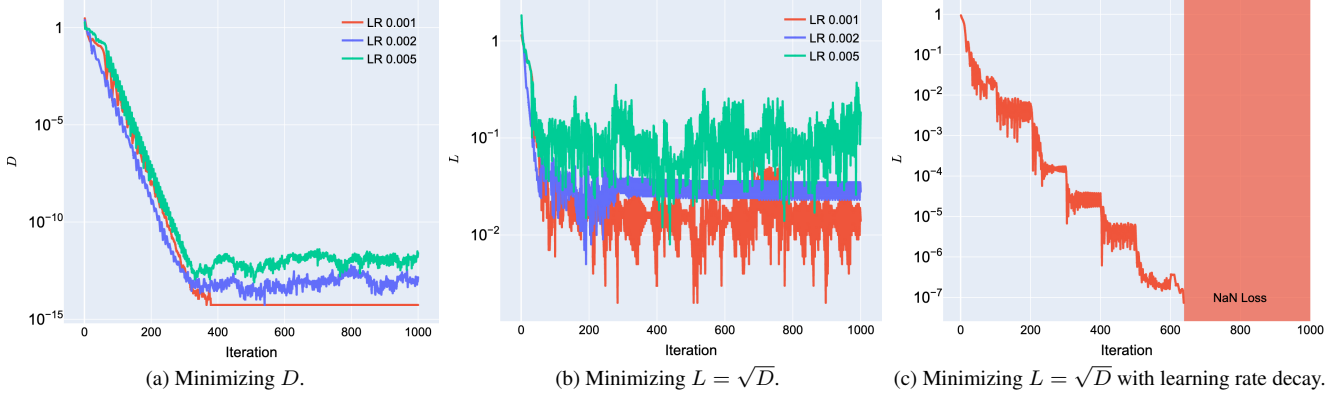


Figure 1. Simulation results comparing the choice of loss.

deviation of the KITTI dataset [13] statistics. We simulated the training of a sigmoid head that received [BatchNorm – ReLU] output as  $\mathbf{x} = \text{ReLU}(\mathbf{B})$  with  $B_i \sim \mathcal{N}(0, 1)$  with its size  $n_h = n_w = 3$ . We configured the last convolutional layer such that it had the following properties: number of channels  $n_{in} = 128$ , kernel size  $k_h = k_w = 3$ , and weight initialization  $W \sim \mathcal{N}(0, 0.1^2)$ . We used a mini-batch size of 10 and the Adam optimizer [21] with learning rates of  $\{0.001, 0.002, 0.005\}$  and 1000 iterations.

First, when using the scale-invariant log loss  $D$ , the loss was sufficiently minimized to less than  $10^{-10}$  (Figure 1a). However, when using the square root loss  $L$ , the optimization did not proceed to a loss below 0.001 (Figure 1b), indicating that employing square root loss hinders optimization.

One may attempt to achieve better optimization by using a learning rate scheduler to reduce the weight updates from a large gradient. Here, we employed a stepwise learning rate scheduler that controls the learning rate starting at 0.001 and decays by 0.1 for every 100 iterations. As shown in Figure 1c, decaying the learning rate helped the optimization against a large gradient and yielded a smaller loss during the early training phase. However, during the late training phase with losses less than  $10^{-7}$ , the NaN loss occurred. This observation is consistent with our analysis that approaching the optimal point causes divergence when using the square root loss.

In summary, the use of the square root loss not only hinders the optimization owing to the large gradient but also causes NaN divergence as the loss approaches zero. In consideration of this observation, we claim the following.

**Guideline 1.** Although the use of the square root loss is beneficial during the early training phase, it causes unstable gradient behavior during the late training phase. If NaN loss is observed during the late training phase, consider not using the square root loss or switching to the original scale-invariant log loss.

## 2.2. Vulnerability in Log-Sigmoid Function

Another vulnerability that causes NaN divergence is the use of a logarithmic function with a sigmoid head. Here, the output distribution of the sigmoid head is significantly affected by the weight initialization of the last convolutional layer. A larger weight scale  $\text{Var}[\mathbf{W}]$  of the last convolutional layer induces a larger scale in  $\mathbf{z}$ , which causes the output of the sigmoid head  $y_i = \text{Ms}(z_i)$  to be polarized to 0 or  $M$ . Note that the resulting value is used for computing  $d_i = \log y_i - \log y_i^*$ , whose logarithmic function is numerically unstable for  $y_i = 0$  since the logarithm of zero is negative infinity. For example, on the FP32 precision of PyTorch [34], the sigmoid function outputs  $s(-88) = 6.0546 \times 10^{-39}$  and  $s(-89) = 0$ . The logarithmic function yields a NaN value for the latter, which leads to the NaN loss. We observed that this scenario occurs in real situations when training a monocular depth estimation network, particularly during the early training phase. To address this problem, we consider two approaches.

### 2.2.1 Approach 1. Weight Initialization

Note that  $z_i$  is obtained by the last convolutional layer of the decoder and is calculated using  $\mathbf{z} = \mathbf{W}\mathbf{x} + b$ . First, it is favorable to achieve a stable scale on the decoder feature  $\text{Var}[\mathbf{x}]$  using an additional batch normalization layer [18] prior to the last ReLU. Although common practices omit the batch normalization layer when computing  $\mathbf{x}$ , we observed that incorporating the batch normalization layer marginally improves the performance and stability. Second, in the case of  $b$ , we observed that the initialization of  $b$  rarely influenced the performance and stability, hence, we used zero initialization following common practice. Finally, because a larger weight scale  $\text{Var}[\mathbf{W}]$  would yield a value such as  $z_i = -89$ , we should set a smaller weight scale.

Note that an initialization of the weight that is too small hinders gradient descent optimization [23, 45, 46]. There-

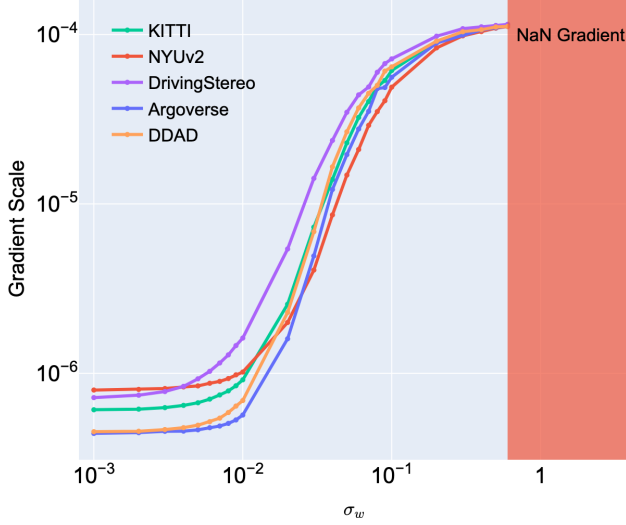


Figure 2. Gradient scale with respect to weight initialization of the last convolutional layer. It should be carefully initialized to achieve a stable gradient scale.

fore, we need to quantify an initialization range that ensures no NaN loss from a small scale on  $\mathbf{z}$  as well as stable behavior in the gradient descent. Here, we simulated the behavior of a sigmoid head by controlling a weight scale to measure its impact on the gradient scale.

**Simulation** We examine whether the gradient scale  $\text{Var}[\partial L / \partial \mathbf{W}]$  would increase or decrease when the weight scale  $\text{Var}[\mathbf{W}]$  increases. Additionally, we monitor the occurrence of NaN loss. We generated artificial random normal data whose ground-truth followed the mean and standard deviation of the {KITTI [13], NYU-Depth V2 [41], Driving Stereo [48], Argoverse [7], DDAD [15]} dataset statistics. We simulated the sigmoid head receiving the [BatchNorm – ReLU] output as  $\mathbf{x} = \text{ReLU}(\mathbf{B})$  with  $B_i \sim \mathcal{N}(0, 1)$  and  $n_h = n_w = 100$ . The last convolutional layer was configured with  $n_{in} = 128$  and  $k_h = k_w = 3$ . A mini-batch size of 10 was used. We measure the gradient scale  $\text{Var}[\partial L / \partial \mathbf{W}]$  by controlling the weight scale  $\text{Var}[\mathbf{W}] = \sigma_W^2$ . Considering randomness, we measure the average of 1,000 simulations.

Figure 2 summarizes the results. Gradient variance is observed to significantly diminish when  $\sigma_W < 0.1$ , which slows down training similar to the vanishing gradient [33]. It should be noted that using the Xavier initialization of  $W \sim \mathcal{N}(0, 2/(k_h k_w (n_{in} + n_{out})))$  [14] yields  $\sigma_W = 0.0415$ , which corresponds to this range and therefore should not be used. In contrast, when  $\sigma_W > 0.6$ , the gradient variance yields a NaN value, which is a result of NaN loss. Stable initialization requires  $0.1 \leq \sigma_W \leq 0.6$ , which we refer to as *stable initialization range*. This range

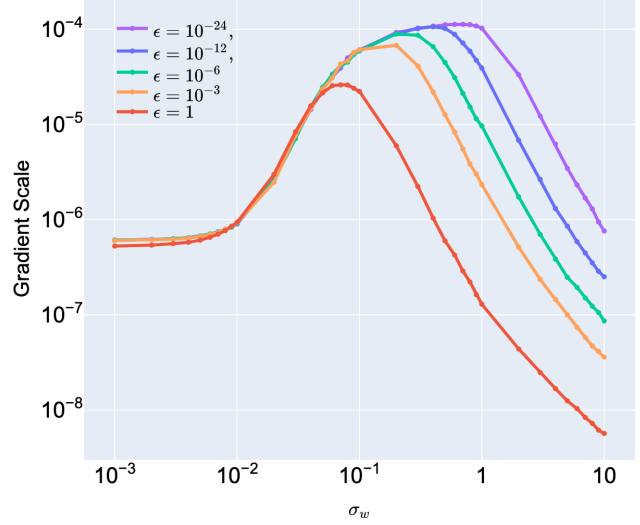


Figure 3. Gradient scale with various choices of  $\epsilon$ . Adding  $\epsilon$  solves the numerical vulnerability of the logarithmic function, unless it is not significantly small such as  $\epsilon \leq 7.0 \times 10^{-46}$ . However, choosing a larger  $\epsilon$  decreases the gradient scale.

can be applied to the aforementioned datasets with one exception: the NYU-Depth V2 dataset requires a slightly higher range of  $0.2 \leq \sigma_W \leq 0.6$ . In Section 3, we demonstrate that weight initialization significantly affects the stability of the optimization as well as the final performance. In summary, the following guidelines are presented:

**Guideline 2-1.** The weight of the last convolutional layer should be carefully initialized. Avoid using common weight initialization, such as Xavier initialization. Ensure the use of a weight initialization within the stable initialization range of  $0.1 \leq \sigma_W \leq 0.6$ .

However, this approach has several limitations. Even though  $\sigma_W \leq 0.6$  is applied at initialization, the weight scale can increase during training, which causes NaN loss. Furthermore, since the active gradient scale is close to this boundary of 0.6, we should consider a trade-off between increasing  $\sigma_W$  to obtain an active gradient and avoiding potential NaN loss.

### 2.2.2 Approach 2. Logarithmic Function

Alternatively, we address this vulnerability by improving the numerical stability of the logarithmic function. When using the logarithmic function, adding a small  $\epsilon > 0$  as  $d_{i,\epsilon} := \log(y_i + \epsilon) - \log(y_i^* + \epsilon)$  ensures that  $y_i + \epsilon > 0$  and solves the numerical problem of the logarithmic function. This practice has been employed in a few implementations of monocular depth estimation models with  $\epsilon = 10^{-3}$  or  $\epsilon = 10^{-6}$  [19, 25, 32, 36], while its importance and validity require more emphasis. Subsequently, we investigated

the validity of this practice.

**Simulation** We used the same simulation setup described above, using the mean and standard deviation of KITTI statistics, but with the addition of  $\epsilon$ . Figure 3 summarizes the gradient variance when using  $\epsilon \in \{1, 10^{-3}, 10^{-6}, 10^{-12}, 10^{-24}\}$ . Furthermore, we observed that  $\epsilon \leq 7.0 \times 10^{-46}$  yielded NaN loss because it was smaller than the representable float (See the Appendix for further details), whereas the five values of  $\epsilon$  resulted in no instances of NaN.

However, choosing a larger  $\epsilon$  decreased the gradient scale. In other words, adding  $\epsilon$  approximates the result as  $d_{i,\epsilon} \approx d_i$ , which affects both the gradient scale and the stable initialization range discussed earlier. In Section 3, we empirically observe that allowing a high gradient scale enhances performance. In consideration of this observation, instead of using  $\epsilon = 10^{-3}$  or  $\epsilon = 10^{-6}$ , as is the current practice, we recommend using a substantially smaller value such as  $\epsilon = 10^{-24}$ . In summary, an active gradient scale requires a substantially smaller  $\epsilon$  with a different stable initialization range. Specifically, we propose the following:

**Guideline 2-2.** Adding  $\epsilon$  solves the numerical issue of the logarithmic function, but the choice of  $\epsilon$  significantly affects the stable initialization range. We recommend using  $\epsilon = 10^{-24}$  and  $0.1 \leq \sigma_W \leq 1$ .

### 2.3. Vulnerability in Variance Computation

Rewriting scale-invariant log loss  $D$ , we obtain

$$D = \frac{1}{n} \sum_i d_i^2 - \frac{\lambda}{n^2} \left( \sum_i d_i \right)^2, \quad (5)$$

$$= E[d^2] - \lambda(E[d])^2 \quad (6)$$

$$= \text{Var}[d] + (1 - \lambda)(E[d])^2. \quad (7)$$

We refer to Eq. 6 as a mean-style implementation and Eq. 7 as a var-style implementation. The two are identical as long as the variance is calculated as the sum of the squared deviations from the mean divided by  $n$ , expressed as:

$$\text{Var}[d] = \frac{1}{n} \sum_i (d_i - E[d])^2. \quad (8)$$

However, for variance computation, modern deep-learning libraries such as PyTorch apply the Bessel correction [38] by default. In other words, `torch.var(x)` is defined as the sum of the squared deviations from the mean divided by  $n - 1$ , expressed as

$$\text{Var}'[d] = \frac{1}{n-1} \sum_i (d_i - E[d])^2, \quad (9)$$

```
1 # Reference: https://github.com/SwinTransformer/
  MIM-Depth-Estimation
2 class SiLogLoss(nn.Module):
3     # ...
4     def forward(self, pred, target):
5         valid_mask = (target > 0).detach()
6         diff_log = torch.log(target[valid_mask])
7         - torch.log(pred[valid_mask])
8         loss = torch.sqrt(torch.pow(diff_log, 2).
  mean() - self.lambd * torch.pow(diff_log.mean
    (), 2))
9         return loss
```

Listing 1. Example of mean-style implementation [47].

```
1 # Reference: https://github.com/zhyever/Monocular
  -Depth-Estimation-Toolbox
2 class SigLoss(nn.Module):
3     # ...
4     def sigloss(self, input, target):
5         # ...
6         g = torch.log(input + self.eps) - torch.
  log(target + self.eps)
7         Dg = torch.var(g) + 0.15 * torch.pow(
  torch.mean(g), 2)
8         return torch.sqrt(Dg)
```

Listing 2. Example of var-style implementation [25].

Mean-Style	Var-Style
MIM [47]	DepthFormer [25]
LapDepth [42]	iDisc [36]
GLPDepth [20]	DDP [19]
D-Net [43]	Depthformer [1]
NeW CRFs [49]	AdaBins [3]
PixelFormer [2]	DINOv2 [32]
VPD [51]	ZeoDepth [5]
AiT [31]	LocalBins [4]

Table 1. Half of the current implementations of monocular depth estimation networks used the mean-style implementation, whereas the other half used the var-style implementation. None of the var-style implementations specifies a biased estimator, which results in incorrect loss computation.

which is also referred to as an unbiased estimator [6]. Thus, when `torch.var(x)` is used, the var-style implementation differs from the mean-style implementation. For example, consider  $\mathbf{d} = \{1, 3\}$  with  $n = 2$  and  $\lambda = 0.5$ . This example yields  $\text{Var}[d] = 1$  and  $\text{Var}'[d] = 2$ , resulting in  $D = 3$  for a biased estimator and  $D = 4$  for an unbiased estimator. To correctly compute the scale-invariant log loss, we should explicitly specify a biased estimator as `torch.var(x, unbiased=False)`.

We examined the current implementations of monocular depth estimation networks. Half of them used the mean-



Valid Pixels	Avg.	Min.	Valid Rate (%)
KITTI [13]	25074	226	20.23
NYU-Depth V2 [41]	173598	6302	75.34
Driving Stereo [48]	31488	778	25.41
Argoverse [7]	1239	0	1.00
DDAD [15]	1489	0	1.20

Table 2. We measured the average and minimum number of valid pixels on cropped images generated during one epoch of training. We observed that the KITTI, NYU-Depth V2, and Driving Stereo datasets provide dense ground-truth depth maps. However, the Argoverse and DDAD datasets provide significantly sparse depth maps with a valid pixel rate of approximately 1%, which can accidentally yield few valid pixels in the cropped image.

style implementation, whereas the other half used the var-style implementation without specifying a biased estimator, which resulted in an incorrect loss computation (Table 1).

When  $n \gg 1$ , the difference between divisions by  $n$  and  $n - 1$  is insignificant. Vulnerability occurs when  $n$  is small, which yields an incorrect loss and gradient. Especially when  $n = 1$ , division by  $n - 1$  causes NaN loss.

Here,  $n$  corresponds to the number of valid pixels during the training. First, valid pixels are dependent on the sparsity of the ground-truth depth map. For example, the ground-truth  $y^*$  of the KITTI dataset was originally measured by a LiDAR scanner of Velodyne HDL-64E that collects sparse 3D points, and other unmeasured areas remain empty [29, 44]. For the monocular depth estimation task, only a small portion of the pixels in  $(n_h \times n_w)$  become valid pixels for use in training, whereas the other invalid pixels are ignored by applying a binary mask. Although the KITTI dataset provides a relatively denser ground-truth, other datasets, such as Argoverse or DDAD, exhibit substantially sparse ground-truth depth maps.

Second, the number of valid pixels is affected by the image crop. During the training of a monocular depth estimation model, several cropping methods, such as KB-crop, random-crop, and Garg-crop [11], are applied in a row to the image and depth map. Owing to the random-crop, the number of valid pixels contained in the ground-truth depth map varies every time. In a long training iteration, the cropped depth map can accidentally contain few valid pixels, such as  $n = 1$  or  $n = 0$ , yielding a NaN loss when using an unbiased estimator of `torch.var(x)`. For sparse datasets such as the Argoverse or DDAD datasets, this phenomenon occurs in real situations (Table 2).

**Simulation** We simulated the impact of sparsity on the variance computation. First, we generate a random depth map of size  $(n_h \times n_w) = (100 \times 100)$  and apply a binary mask to obtain a sparse

Valid Rate (%)	# of NaNs for <code>torch.var(x)</code>	
	Default	unbiased=False
0.05	457	92
0.06	229	30
0.07	89	8
0.08	35	5
0.09	19	1
0.10	9	1
0.11	2	0
0.12	1	0
0.13	0	0
0.14	0	0

Table 3. Number of NaN occurrences with respect to the sparsity of valid pixels. The default option leads to an unbiased estimator and is vulnerable to  $n = 1$  and  $n = 0$ , whereas specifying a biased estimator is only vulnerable to  $n = 0$ , which can be passed in practice by checking the sanity of the depth map.

depth map. Controlling its sparsity, we counted the number of NaNs when using `torch.var(x)` and `torch.var(x, unbiased=False)` on 10,000 simulations.

Table 3 summarizes the result. Generally, NaN is encountered only in cases of severe sparsity. We observed that when the rate of valid pixels was lower than 0.12%, the variance computation began to yield NaN. Note that `torch.var(x)` results in NaN for  $n = 1$  or  $n = 0$ , whereas `torch.var(x, unbiased=False)` yields NaN only for  $n = 0$ , which can be passed in practice by verifying the sanity of the depth map. Because of this difference, `torch.var(x)` is vulnerable to NaN loss. In consideration of this vulnerability, we claim the following:

**Guideline 3.** We recommend using the mean-style implementation of scale-invariant log loss. When using the var-style implementation, do specify a biased estimator to obtain the correct results. Ensure skipping for  $n = 0$  by using a conditional statement.

### 3. Experiments

**Objective** In the previous section, we demonstrated the occurrence of NaN loss in each of three vulnerabilities. Meanwhile, in the previous section, we claimed that allowing a high gradient scale enhances the performance of monocular depth estimation. To validate this claim, experiments were conducted with an extensive range of weight initializations. We pursued an investigation of the validity rather than hyperparameter tuning. The main objective of this study is to analyze and solve the problem of NaN loss. Achieving state-of-the-art performance is beyond the scope of this study.

Dataset	$\epsilon$	$\sigma_W$	$\delta < 1.25 \uparrow$	$\delta < 1.25^2 \uparrow$	$\delta < 1.25^3 \uparrow$	Abs Rel $\downarrow$	Sq Rel $\downarrow$	RMSE $\downarrow$	RMSE log $\downarrow$	log10 $\downarrow$
K	0	0.001*	0.9751	0.9974	0.9994	0.0514	0.1489	2.0690	0.0779	0.0224
		0.002	0.9755	0.9974	0.9994	0.0514	0.1479	2.0628	0.0778	0.0225
		0.005	0.9754	0.9974	0.9993	0.0513	0.1484	2.0644	0.0776	0.0223
		0.01	0.9755	<b>0.9975</b>	0.9994	0.0510	0.1469	2.0572	0.0772	0.0223
		0.02	0.9757	0.9974	0.9994	0.0511	0.1466	2.0549	0.0774	0.0223
		0.05	0.9755	0.9974	0.9994	0.0514	0.1472	2.0475	0.0776	0.0224
		0.1	<b>0.9761</b>	0.9973	0.9994	<b>0.0508</b>	<b>0.1454</b>	<b>2.0226</b>	<b>0.0767</b>	<b>0.0221</b>
		0.2	0.9756	0.9974	0.9994	0.0510	0.1467	2.0603	0.0774	0.0223
		0.5	0.9745	0.9974	0.9994	0.0518	0.1494	2.0809	0.0783	0.0227
		1				NaN				
		2				NaN				
		5				NaN				
		10				NaN				
K	$10^{-24}$	0.001	0.9756	0.9974	0.9994	0.0520	0.1482	2.0616	0.0778	0.0226
		0.002	0.9756	0.9974	0.9994	0.0514	0.1475	2.0385	0.0771	<b>0.0222</b>
		0.005	0.9754	0.9974	0.9993	0.0512	0.1474	2.0526	0.0776	0.0224
		0.01	0.9757	<b>0.9975</b>	0.9994	0.0515	0.1463	2.0412	0.0772	0.0224
		0.02	0.9758	<b>0.9975</b>	0.9994	0.0509	0.1459	2.0538	<b>0.0770</b>	<b>0.0222</b>
		0.05	0.9750	0.9974	0.9994	0.0517	0.1480	2.0525	0.0778	0.0225
		0.1	<b>0.9759</b>	<b>0.9975</b>	0.9993	0.0515	0.1469	2.0452	0.0775	0.0224
		0.2	0.9758	0.9974	0.9994	0.0510	0.1469	2.0494	0.0773	0.0223
		0.5	0.9757	0.9974	0.9994	<b>0.0508</b>	<b>0.1458</b>	<b>2.0373</b>	<b>0.0770</b>	<b>0.0222</b>
		1	0.9751	0.9974	0.9994	0.0515	0.1476	2.0583	0.0778	0.0225
		2	0.9736	0.9971	0.9993	0.0545	0.1558	2.1027	0.0806	0.0238
		5	0.9721	0.9968	0.9992	0.0570	0.1638	2.1590	0.0835	0.0250
		10	0.0070	0.0198	0.0402	6.4862	453.7119	66.0504	1.9510	0.8128
N	0	0.001*	0.9317	0.9909	0.9980	0.0920	0.0449	0.3120	0.1124	0.0383
		0.002	0.9339	0.9911	0.9979	0.0905	0.0460	0.3103	0.1113	0.0378
		0.005	0.9338	0.9913	0.9981	0.0899	0.0443	0.3082	0.1110	0.0375
		0.01	0.9342	0.9913	0.9979	0.0895	0.0451	0.3092	0.1107	0.0374
		0.02	0.9347	0.9911	0.9980	0.0896	0.0447	0.3076	0.1107	0.0374
		0.05	0.9335	0.9914	0.9981	0.0892	0.0447	0.3074	0.1104	0.0373
		0.1	0.9345	0.9911	0.9980	0.0897	0.0448	0.3081	0.1108	0.0374
		0.2	<b>0.9352</b>	<b>0.9915</b>	0.9981	<b>0.0883</b>	<b>0.0439</b>	<b>0.3072</b>	<b>0.1098</b>	<b>0.0371</b>
		0.5				NaN				
		1				NaN				
		2				NaN				
		5				NaN				
		10				NaN				
N	$10^{-24}$	0.001	0.9331	0.9907	0.9980	0.0917	0.0460	0.3132	0.1123	0.0382
		0.002	0.9325	0.9914	0.9980	0.0911	0.0452	0.3109	0.1119	0.0380
		0.005	0.9315	0.9912	0.9980	0.0922	0.0456	0.3122	0.1126	0.0383
		0.01	0.9317	0.9910	0.9981	0.0919	0.0451	0.3124	0.1126	0.0382
		0.02	0.9343	0.9906	0.9980	0.0899	0.0446	0.3093	0.1111	0.0376
		0.05	0.9333	0.9910	0.9980	0.0893	0.0443	0.3075	0.1107	0.0374
		0.1	0.9335	0.9911	0.9980	0.0894	0.0450	0.3088	0.1107	0.0374
		0.2	0.9356	0.9910	0.9981	0.0876	<b>0.0430</b>	<b>0.3045</b>	0.1094	0.0369
		0.5	<b>0.9361</b>	<b>0.9916</b>	0.9981	<b>0.0864</b>	0.0435	0.3046	<b>0.1088</b>	<b>0.0365</b>
		1	0.9340	0.9910	0.9980	0.0888	0.0446	0.3073	0.1105	0.0372
		2	0.9296	0.9909	0.9981	0.0907	0.0450	0.3130	0.1129	0.0381
		5	0.3129	0.3424	0.3679	2.4012	18.8513	5.0322	1.0141	0.4224
		10	0.2678	0.3328	0.3660	2.4188	18.8605	5.0928	1.0367	0.4304

Table 4. Experimental results of monocular depth estimation. Here, “K” denotes KITTI and “N” denotes NYU-Depth V2. \* indicates the baseline.

### 3.1. Implementation Details

**Target model** used in this study was the model studied by masked image modeling (MIM), which has recently achieved state-of-the-art performance in the monocular depth estimation task [47]. The MIM successfully trained the SwinV2-Base [27] to achieve improved performance, which served as the pretrained backbone for the encoder of the monocular depth estimation network. We implemented the MIM using the official GitHub repository. Note that the official MIM implementation used weight initialization  $\sigma_W = 0.001$  without adding  $\epsilon$ ; hence, we examined whether their weight initialization can be further improved in terms of stability and performance.

**Hyperparameters** We used the AdamW optimizer [28] with  $\beta_1 = 0.9$ ,  $\beta_2 = 0.999$  and weight decay  $5 \times 10^{-2}$ , learning rate scheduler of polynomial decay using factor 0.9 and its maximum  $5 \times 10^{-4}$  to minimum  $3 \times 10^{-5}$ , and number of epochs 25. The average of three runs with different random seeds is reported for each result. Training was conducted using a 4×A100 GPU machine.

**Evaluation metrics** We used the following evaluation metrics commonly used in the monocular depth estimation tasks:

- Threshold: % of  $y_i$  s.t.  $\max(y_i/y_i^*, y_i^*/y_i) = \delta < thr$ ,
- Abs Rel:  $\frac{1}{n} \sum_i |y_i - y_i^*|/y_i^*$ ,
- Sq Rel:  $\frac{1}{n} \sum_i (y_i - y_i^*)^2/y_i^*$ ,
- RMSE:  $\sqrt{\frac{1}{n} \sum_i (y_i - y_i^*)^2}$ ,
- RMSE log:  $\sqrt{\frac{1}{n} \sum_i (\log y_i - \log y_i^*)^2}$ ,
- log10:  $\frac{1}{n} \sum_i |\log_{10} y_i - \log_{10} y_i^*|$ .

Higher is better for the threshold metric, whereas lower is better for the other five metrics.

**KITTI** dataset contains RGB images and the corresponding ground truth depth maps. The ground truth depth map was measured using a LiDAR scanner that collected sparse 3D points; the other unmeasured areas remained empty. In the KITTI dataset, the maximum depth was  $M = 80$ . The KITTI dataset provides ground truth depth maps with an average valid pixel rate of approximately 20% (Table 2). The size of the original image was  $1241 \times 376$ , which was cropped by KB-crop, random-crop, and Garg-crop during training to obtain a  $352 \times 352$  image and a depth map.

**NYU-Depth V2** dataset contains RGB images and their corresponding depth maps. The dataset was obtained from indoor scenes using a Microsoft Kinect, which provided dense ground truth depth maps with a valid pixel rate of approximately 75%. For the NYU-Depth V2 dataset, the

maximum depth was  $M = 10$ . Following existing MIM practices, we used a  $480 \times 480$  crop for training.

### 3.2. Experimental Results

We set the last convolutional layer to  $n_{in} = 128$ ,  $n_{out} = 1$ , and  $k_h = k_w = 3$ . For Xavier initialization of  $W \sim \mathcal{N}(0, 2/(k_h k_w (n_{in} + n_{out})))$ , we obtain  $\sigma_W = 0.0415$ , while He initialization of  $W \sim \mathcal{N}(0, 2/(k_h k_w n_{out}))$  [16] yields  $\sigma_W = 0.4714$ . However, it was observed that the best initialization could differ substantially from the two initializations, depending on the experimental setup.

We examined the effects of weight initialization. The first and third blocks of Table 4 summarize the results with  $\epsilon = 0$ . We observed NaN loss when  $\sigma_W \geq 1$  for KITTI. For NYU-Depth V2, it was observed that NaN loss occurred when using the initialization of  $\sigma_W \geq 0.5$ , which indicates that weight scale increased during training. Note that He initialization was close to this borderline. The best performance was observed at  $\sigma_W = 0.1$  for KITTI and  $\sigma_W = 0.2$  for NYU-Depth V2. Note that the latter is close to the NaN borderline of  $\sigma_W = 0.5$ , and thus when using  $\epsilon = 0$ , we should consider a trade-off between increasing  $\sigma_W$  to obtain an active gradient and avoiding potential NaN loss.

We investigated the effect of adding  $\epsilon = 10^{-24}$ . The second and fourth blocks of Table 4 summarize the results. Here no cases of NaN were observed, even in the previous NaN borderline of  $\sigma_W = 0.5$  or  $\sigma_W = 1$ . Therefore, we can enjoy increasing  $\sigma_W$  to obtain an active gradient without any potential NaN loss. However, as we described in the previous section, the stable initialization range changed by adding  $\epsilon$ . The best performance was obtained at a larger weight initialization of  $\sigma_W = 0.5$  for KITTI and  $\sigma_W = 0.2$  or  $\sigma_W = 0.5$  for NYU-Depth V2.

## 4. Conclusion

This study discussed three vulnerabilities in monocular depth estimation training. First, we found that the square root loss resulted in unstable gradient scaling. Vulnerability was found to cause NaN loss during the late training phase where we recommended using the original scale-invariant log loss. Second, we determined that the log-sigmoid function has numerical problems. The occurrence of NaN loss was demonstrated by module tests involving the log-sigmoid function, and two possible solutions were suggested. Finally, we revealed that half of the current implementations of the scale-invariant log loss yielded incorrect results owing to the use of an unbiased estimator. Because this problem can accidentally cause NaN loss in a sparse depth map, we claimed to use a biased estimator to ensure the correct result. Through experiments, we validated that the proposed guidelines improved optimization stability. We hope that our guidelines for obtaining stable optimization will aid the research community of monocular depth estimation.



## References

- [1] Ashutosh Agarwal and Chetan Arora. Depthformer: Multiscale Vision Transformer for Monocular Depth Estimation with Global Local Information Fusion. In *ICIP*, pages 3873–3877, 2022. 5
- [2] Ashutosh Agarwal and Chetan Arora. Attention Attention Everywhere: Monocular Depth Prediction with Skip Attention. In *WACV*, pages 5850–5859, 2023. 5
- [3] Shariq Farooq Bhat, Ibraheem Alhashim, and Peter Wonka. AdaBins: Depth Estimation Using Adaptive Bins. In *CVPR*, pages 4009–4018, 2021. 5
- [4] Shariq Farooq Bhat, Ibraheem Alhashim, and Peter Wonka. LocalBins: Improving Depth Estimation by Learning Local Distributions. In *ECCV (I)*, pages 480–496, 2022. 5
- [5] Shariq Farooq Bhat, Reiner Birkel, Diana Wofk, Peter Wonka, and Matthias Müller. ZoeDepth: Zero-shot Transfer by Combining Relative and Metric Depth. *CoRR*, abs/2302.12288, 2023. 5
- [6] George W Brown. On small-sample estimation. *The Annals of Mathematical Statistics*, 18(4):582–585, 1947. 5
- [7] Ming-Fang Chang, John Lambert, Patsorn Sangkloy, Jagjeet Singh, Slawomir Bak, Andrew Hartnett, De Wang, Peter Carr, Simon Lucey, Deva Ramanan, and James Hays. Argoverse: 3D Tracking and Forecasting With Rich Maps. In *CVPR*, pages 8748–8757, 2019. 4, 6
- [8] Liang-Chieh Chen, Yukun Zhu, George Papandreou, Florian Schroff, and Hartwig Adam. Encoder-Decoder with Atrous Separable Convolution for Semantic Image Segmentation. In *ECCV (7)*, pages 833–851, 2018. 1
- [9] Alexey Dosovitskiy, Lucas Beyer, Alexander Kolesnikov, Dirk Weissenborn, Xiaohua Zhai, Thomas Unterthiner, Mostafa Dehghani, Matthias Minderer, Georg Heigold, Sylvain Gelly, Jakob Uszkoreit, and Neil Houlsby. An Image is Worth 16x16 Words: Transformers for Image Recognition at Scale. In *ICLR*, 2021. 1
- [10] David Eigen, Christian Puhrsch, and Rob Fergus. Depth Map Prediction from a Single Image using a Multi-Scale Deep Network. In *NIPS*, pages 2366–2374, 2014. 2
- [11] Ravi Garg, B. G. Vijay Kumar, Gustavo Carneiro, and Ian D. Reid. Unsupervised CNN for Single View Depth Estimation: Geometry to the Rescue. In *ECCV (8)*, pages 740–756, 2016. 6
- [12] Timur Garipov, Pavel Izmailov, Dmitrii Podoprikin, Dmitry P. Vetrov, and Andrew Gordon Wilson. Loss Surfaces, Mode Connectivity, and Fast Ensembling of DNNs. In *NeurIPS*, pages 8803–8812, 2018. 2
- [13] Andreas Geiger, Philip Lenz, Christoph Stiller, and Raquel Urtasun. Vision meets robotics: The KITTI dataset. *Int. J. Robotics Res.*, 32(11):1231–1237, 2013. 3, 4, 6
- [14] Xavier Glorot and Yoshua Bengio. Understanding the difficulty of training deep feedforward neural networks. In *AISTATS*, pages 249–256, 2010. 4
- [15] Vitor Guizilini, Rares Ambrus, Sudeep Pillai, Allan Raventos, and Adrien Gaidon. 3D Packing for Self-Supervised Monocular Depth Estimation. In *CVPR*, pages 2482–2491, 2020. 4, 6
- [16] Kaiming He, Xiangyu Zhang, Shaoqing Ren, and Jian Sun. Delving Deep into Rectifiers: Surpassing Human-Level Performance on ImageNet Classification. In *ICCV*, pages 1026–1034, 2015. 8
- [17] Kaiming He, Xiangyu Zhang, Shaoqing Ren, and Jian Sun. Deep Residual Learning for Image Recognition. In *CVPR*, pages 770–778, 2016. 1
- [18] Sergey Ioffe and Christian Szegedy. Batch Normalization: Accelerating Deep Network Training by Reducing Internal Covariate Shift. In *ICML*, pages 448–456, 2015. 3
- [19] Yuanfeng Ji, Zhe Chen, Enze Xie, Lanqing Hong, Xihui Liu, Zhaoqiang Liu, Tong Lu, Zhenguo Li, and Ping Luo. DDP: Diffusion Model for Dense Visual Prediction. *CoRR*, abs/2303.17559, 2023. 4, 5
- [20] Doyeon Kim, Woonghyun Ga, Pyunghwan Ahn, Donggyu Joo, Sewhan Chun, and Junmo Kim. Global-Local Path Networks for Monocular Depth Estimation with Vertical Cut-Depth. *CoRR*, abs/2201.07436, 2022. 5
- [21] Diederik P. Kingma and Jimmy Ba. Adam: A Method for Stochastic Optimization. In *ICLR*, 2015. 3
- [22] Jin Han Lee, Myung-Kyu Han, Dong Wook Ko, and Il Hong Suh. From Big to Small: Multi-Scale Local Planar Guidance for Monocular Depth Estimation. *CoRR*, abs/1907.10326, 2019. 2
- [23] Aitor Lewkowycz and Guy Gur-Ari. On the training dynamics of deep networks with L2 regularization. In *NeurIPS*, 2020. 3
- [24] Hao Li, Zheng Xu, Gavin Taylor, Christoph Studer, and Tom Goldstein. Visualizing the Loss Landscape of Neural Nets. In *NeurIPS*, pages 6391–6401, 2018. 2
- [25] Zhenyu Li, Zehui Chen, Xianming Liu, and Junjun Jiang. DepthFormer: Exploiting Long-Range Correlation and Local Information for Accurate Monocular Depth Estimation. *Machine Intelligence Research*, 2023. 4, 5
- [26] Ce Liu, Suryansh Kumar, Shuhang Gu, Radu Timofte, and Luc Van Gool. VA-DepthNet: A Variational Approach to Single Image Depth Prediction. In *ICLR*, 2023. 2
- [27] Ze Liu, Han Hu, Yutong Lin, Zhuliang Yao, Zhenda Xie, Yixuan Wei, Jia Ning, Yue Cao, Zheng Zhang, Li Dong, Furu Wei, and Baining Guo. Swin Transformer V2: Scaling Up Capacity and Resolution. In *CVPR*, pages 11999–12009, 2022. 8
- [28] Ilya Loshchilov and Frank Hutter. Decoupled Weight Decay Regularization. In *ICLR*, 2019. 8
- [29] Will Maddern and Paul M. Newman. Real-time probabilistic fusion of sparse 3D LIDAR and dense stereo. In *IROS*, pages 2181–2188, 2016. 6
- [30] Gouthamaan Manimaran and J Swaminathan. Focal-WNet: An Architecture Unifying Convolution and Attention for Depth Estimation. In *2022 IEEE 7th International conference for Convergence in Technology (I2CT)*, pages 1–7, 2022. 2
- [31] Jia Ning, Chen Li, Zheng Zhang, Zigang Geng, Qi Dai, Kun He, and Han Hu. All in Tokens: Unifying Output Space of Visual Tasks via Soft Token. *CoRR*, abs/2301.02229, 2023. 5

- [32] Maxime Oquab, Timothée Darcet, Théo Moutakanni, Huy Vo, Marc Szafraniec, Vasil Khalidov, Pierre Fernandez, Daniel Haziza, Francisco Massa, Alaaeldin El-Nouby, Mahmoud Assran, Nicolas Ballas, Wojciech Galuba, Russell Howes, Po-Yao Huang, Shang-Wen Li, Ishan Misra, Michael G. Rabbat, Vasu Sharma, Gabriel Synnaeve, Hu Xu, Hervé Jégou, Julien Mairal, Patrick Labatut, Armand Joulin, and Piotr Bojanowski. DINOv2: Learning Robust Visual Features without Supervision. *CoRR*, abs/2304.07193, 2023. 4, 5
- [33] Razvan Pascanu, Tomás Mikolov, and Yoshua Bengio. On the difficulty of training recurrent neural networks. In *ICML* (3), pages 1310–1318, 2013. 2, 4
- [34] Adam Paszke, Sam Gross, Francisco Massa, Adam Lerer, James Bradbury, Gregory Chanan, Trevor Killeen, Zeming Lin, Natalia Gimelshein, Luca Antiga, Alban Desmaison, Andreas Köpf, Edward Z. Yang, Zachary DeVito, Martin Raison, Alykhan Tejani, Sasank Chilamkurthy, Benoit Steiner, Lu Fang, Junjie Bai, and Soumith Chintala. PyTorch: An Imperative Style, High-Performance Deep Learning Library. In *NeurIPS*, pages 8024–8035, 2019. 3
- [35] Vaishakh Patil, Christos Sakaridis, Alexander Liniger, and Luc Van Gool. P3Depth: Monocular Depth Estimation with a Piecewise Planarity Prior. In *CVPR*, pages 1600–1611, 2022. 2
- [36] Luigi Piccinelli, Christos Sakaridis, and Fisher Yu. iDisc: Internal Discretization for Monocular Depth Estimation. In *CVPR*, pages 21477–21487, 2023. 4, 5
- [37] René Ranftl, Alexey Bochkovskiy, and Vladlen Koltun. Vision Transformers for Dense Prediction. In *ICCV*, pages 12159–12168, 2021. 1
- [38] William John Reichmann. Use and abuse of statistics. 1961. 5
- [39] Shuwei Shao, Zhongcai Pei, Weihai Chen, Ran Li, Zhong Liu, and Zhengguo Li. URCD-Depth: Uncertainty Rectified Cross-Distillation with CutFlip for Monocular Depth Estimation. *CoRR*, abs/2302.08149, 2023. 2
- [40] Shuwei Shao, Zhongcai Pei, Xingming Wu, Zhong Liu, Weihai Chen, and Zhengguo Li. IEBins: Iterative Elastic Bins for Monocular Depth Estimation. In *NeurIPS*, 2023. 2
- [41] Nathan Silberman, Derek Hoiem, Pushmeet Kohli, and Rob Fergus. Indoor Segmentation and Support Inference from RGBD Images. In *ECCV* (5), pages 746–760, 2012. 4, 6
- [42] Minsoo Song, Seokjae Lim, and Wonjun Kim. Monocular Depth Estimation Using Laplacian Pyramid-Based Depth Residuals. *IEEE Trans. Circuits Syst. Video Technol.*, 31(11): 4381–4393, 2021. 5
- [43] Joshua Luke Thompson, Son Lam Phung, and Abdesselam Bouzerdoum. D-Net: A Generalised and Optimised Deep Network for Monocular Depth Estimation. *IEEE Access*, 9: 134543–134555, 2021. 5
- [44] Jonas Uhrig, Nick Schneider, Lukas Schneider, Uwe Franke, Thomas Brox, and Andreas Geiger. Sparsity Invariant CNNs. In *3DV*, pages 11–20, 2017. 6
- [45] Twan van Laarhoven. L2 Regularization versus Batch and Weight Normalization. *CoRR*, abs/1706.05350, 2017. 3
- [46] Zeke Xie, Issei Sato, and Masashi Sugiyama. Stable Weight Decay Regularization. *CoRR*, abs/2011.11152, 2020. 3
- [47] Zhenda Xie, Zigang Geng, Jingcheng Hu, Zheng Zhang, Han Hu, and Yue Cao. Revealing the Dark Secrets of Masked Image Modeling. In *CVPR*, pages 14475–14485, 2023. 5, 8
- [48] Guorun Yang, Xiao Song, Chaoqin Huang, Zhidong Deng, Jianping Shi, and Bolei Zhou. DrivingStereo: A Large-Scale Dataset for Stereo Matching in Autonomous Driving Scenarios. In *CVPR*, pages 899–908, 2019. 4, 6
- [49] Weihao Yuan, Xiaodong Gu, Zuozhuo Dai, Siyu Zhu, and Ping Tan. Neural Window Fully-connected CRFs for Monocular Depth Estimation. In *CVPR*, pages 3906–3915, 2022. 5
- [50] Jingzhao Zhang, Tianxing He, Suvrit Sra, and Ali Jadbabaie. Why Gradient Clipping Accelerates Training: A Theoretical Justification for Adaptivity. In *ICLR*, 2020. 2
- [51] Wenliang Zhao, Yongming Rao, Zuyan Liu, Benlin Liu, Jie Zhou, and Jiwen Lu. Unleashing Text-to-Image Diffusion Models for Visual Perception. In *ICCV*, 2023. 5